HEFAT2010
7th International Conference on Heat Transfer, Fluid Mechanics and Thermodynamics
19-21 July 2010
Antalya, Turkey

A CFD STUDY OF NON-NEWTONIAN OIL SAND TAILINGS FLOW IN FUNNEL GEOMETRIES

Kirpalani D.M.[a *], R. Mikula[b] and A. Demoz[b]
*Author for correspondence

[a] Institute for Chemical Process and Environmental Technology
National Research Council of Canada
Ottawa, ON, Canada

[b] CANMET Energy Technology Centre (CETC-Devon), Devon, Alberta
1 Oil Patch Dr. Devon, AB T9G 1A8 CA

ABSTRACT

The bituminous oil sands formations in northern Alberta, Canada are a vital economic natural resource for Canada as their potential for oil production has become quite relevant in recent years due to advances in petrochemical technology. However, the disposal of slurries from the synthetic oil production processes has become quite problematic and addressing this issue is of paramount importance in order to preserve the sensitive ecosystems in this area. These slurries are also known as oil sands tailings, and composed of coarse, fine and mature fine tailings (partially processed).

The focus of this paper is on the flow characteristics of mature fine tailings since they possess poor consolidation properties and take a very long time, often decades, to settle as compared with coarse tailings. Due to the chemical composition of the oil sands tailings, their rheological characteristics are extremely complex. Therefore, a theoretical study of their flow properties with simple test geometries that is valuable in gaining an understanding of the settling process dynamics is performed in this work. The model development was carried out using a commercial computational fluid dynamics (CFD) package FLUENT (version 6.3) and validated with empirical data for further development of processes for tailings transfer and settling with minimal disturbance.

INTRODUCTION

The bituminous oil sands formations in northern Alberta are a vital economic natural resource for Canada as their potential for oil production has become quite lucrative in recent years due to advances in petrochemical technology. These oil reserves' capacity in the energy market is undoubtedly enormous. Unfortunately, the disposal of slurry wastes from the synthetic oil production processes has become quite problematic [4] and addressing this issue is of paramount importance in order to preserve the sensitive ecosystems in this area. These slurry wastes are also known as oil sands tailings, and they can be classified into three categories: coarse tailings, fine tailings, and partially processed mature fine tailings. The focus of this project is on the flow characteristics of mature fine tailings. They are known to have poor consolidation properties and take a very long time, often decades, to settle [4]. On the other hand, coarse tailings settle out quickly and form the containment dykes/berms of the settling basin [5]. Oil companies currently deposit them in large reservoirs known as tailing pond dykes [5].

NON-NEWTONIAN FLUID FLOW BEHAVIOUR

Shearing is one mechanism of momentum transport in a fluid. Consider a fluid between a stationary plate and a moving plate, as in Figure 1. When the fluid moves, it feels resistance due to the velocity differences between its layers. The basic premise of a Newtonian fluid is that, for laminar flow, the shear stress is proportional to velocity gradient in the direction perpendicular to the fluid layers. This gradient is known as the shear rate, and the constant of proportionality is called viscosity.

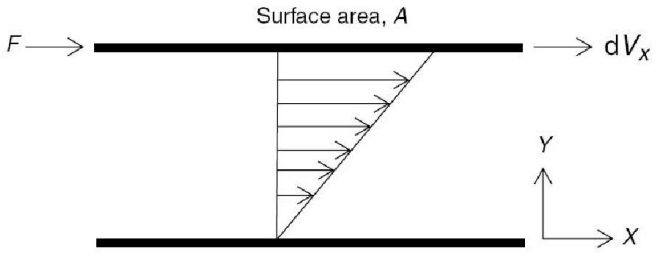

Figure 1: Fluid undergoing unidirectional shear under laminar flow conditions [1]

$$\frac{F}{A} = \tau = \mu\left(-\frac{\partial v}{\partial y}\right) = \mu\dot{\gamma} \quad (1)$$

where F is the applied force (N), A is the surface area of the plate (m^2), τ is the shear stress (Pa), μ is the viscosity (Pa·s), v is the velocity field (m/s) representing the laminar flow, and $\dot{\gamma}$

is the shear rate (1/s). The negative signifies the fluid resistance to the applied force) [1].

This model holds for a large variety of fluids such as water, vegetable oil and alcohol, but does not describe the peculiar behaviour of fluids such as honey, ketchup, cornstarch solutions or molten chocolate. Hence, one requires a more advanced formalism to describe the behaviour of such fluids or mature fine tailings. For such fluids, the viscosity may vary with shear rate or even depend on the shear history. Fluids which have a variable viscosity (i.e. a complex nonlinear relationship to other variables) are termed non-Newtonian fluids. Figure 2 depicts the various classes of non-Newtonian fluids (note the hysteresis for the time-dependent fluids).

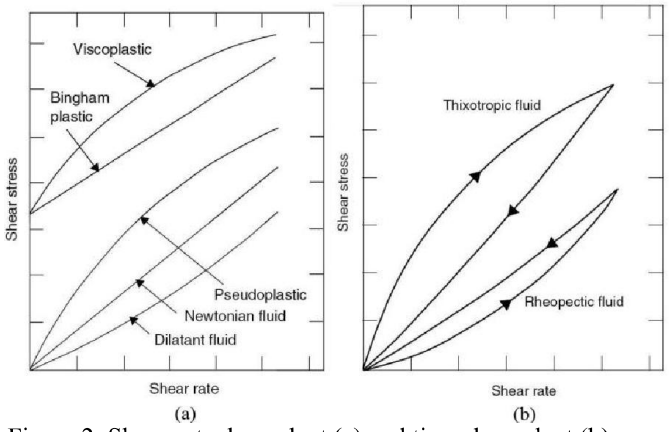

Figure 2: Shear-rate dependent (a) and time-dependent (b) non-Newtonian fluids [1]

Oil sands tailings form cake-like solids when allowed to stand, but flow freely when there is an applied shear stress. It is postulated that these fluids fall into the category of thixotropic fluids (time-dependent data is not available to confirm this, but physical intuition suggests that they would not exhibit rheopecty). The fluid's composition is chiefly responsible for this behaviour as the fine particulates form a very stable and fine dispersion that makes separation very difficult. Recent evidence seems to suggest that the fluid is both shear rate dependent as well as time dependent [4]. Therefore, it is thought that both time-dependent models as well as shear-rate dependent models must be coupled for a more complete description of the non-Newtonian fluid.

However, we will only consider the shear-rate dependence here for simplicity and because time-dependent data is unavailable. Many empirical models have been proposed to explicitly address this shear-rate dependence. One model, known as the Herschel-Bulkley model, is especially useful as it combines the properties of several other models into a more generalized, flexible structure. The model's flexibility manifests itself via the combination of the concepts of yield stress and nonlinear power-law dependence. Naturally, the drawback is the increased number of free parameters. The equation for this model is given on the next page [1]:

$$\tau = \tau_0 + k\dot{\gamma}^n \qquad (2)$$

where τ is the shear stress (Pa), τ_0 is the yield stress (Pa), k is the fluid consistency parameter (Pa·s^n), $\dot{\gamma}$ is the shear rate (1/s) and n is the power law index (dimensionless). The $\tau - \dot{\gamma}$ curve for this model resembles the visco-plastic curve in Figure 2 when all the free parameters (τ_0, k, n) are nonzero. Please see Appendix A, for more information on the process of nonlinear regression applied to available material data and the final Herschel-Bulkley parameters obtained for mature fine tailings samples of various solids contents.

Solving any fluid dynamics problem usually involves treatment of the conservation equations, such as mass, momentum and energy. For our case, we consider mass and momentum equations for a control volume (CV). They are presented below [6,7].

$$\frac{\partial \rho}{\partial t} = -\nabla \cdot (\rho \mathbf{v}) \qquad (3)$$

$$\frac{D\mathbf{v}}{Dt} = -\frac{1}{\rho}\nabla p + \nu \nabla^2 \mathbf{v} + \mathbf{f} \qquad (4)$$

where ρ is a scalar density field, $\mathbf{v}$ is the velocity field, p is the scalar pressure field, ν is the kinematic viscosity, and $\mathbf{f}$ represents body forces acting on the control volume, normalized by the density. $\frac{D()}{Dt}$ is the substantial derivative given by $\frac{\partial()}{\partial t} + \mathbf{v} \cdot \nabla(\ )$.

The first equation is known as the continuity equation, and its physical translation suggests that any net outflow of matter from the control volume constitutes a time-dependent decrease (reason for negative sign) in density within that control volume. The second equation, known as the Navier-Stokes equation, is a momentum conservation applied to an ensemble of infinitesimal fluid elements, and in fact reduces to Newton's second law for a control volume if dimensional analysis is applied.

As our problem deals with an incompressible fluid, it is important to realize that the continuity equation simplifies to:

$$\nabla \cdot \mathbf{v} = 0 \qquad (5)$$

This equation, along with the Navier-Stokes equation is the governing equations for fluid flow in our problem. Note that the viscosity parameter will be variable instead of constant due to the inherent nature of the non-Newtonian fluid. However, these transport equations still do not address the existence of two phases and problem of interface tracking. This requires another mathematical framework known as the volume of fluid (VOF) method, which will be discussed in the next section.

MULTIPHASE SIMULATION

Numerous methods exist for tracking of interfaces in multiphase flow include; the front tracking method, boundary integral method, volume of fluid method, Lattice Boltzmann

method, diffuse interface modelling, and the level set method [8]. The volume of fluid (VOF) method was chosen for this set of simulations, as that was the most appropriate method available in FLUENT.

There are several key components to the VOF implementation, among them is the definition of the colour function and the concept of interfacial geometry reconstruction. The colour function C is defined on a computational grid as the volume fraction (sometimes written as ϕ) of the liquid phase in each cell (position indices i, j, k). In fact, it is the direct discrete analog of the continuous characteristic function $\chi(x, y, z)$ that gives the volume fraction at every point in space. This is definition is summarized in the equation below for a regular hexahedral cell (all side lengths equal to h) [2].

$$C_{ijk}h^3 \approx \iiint_{ijk} \chi(x,y,z)\,\mathrm{d}x\mathrm{d}y\mathrm{d}z \qquad (6)$$

Naturally, this colour function must obey some conservation law so that it is a realistic representation of the moving interface. One of the equations it must satisfy is the advection equation, presented below [9]. This equation basically states that the interface must be transported along with the fluid elements. The discrete form of this equation provides the basis for interface propagation in the VOF algorithm[2].

$$\frac{\partial C}{\partial t} + \mathbf{v}\cdot\nabla C = 0 \qquad (7)$$

The second part of the VOF algorithm involves reconstruction. This is actually quite a difficult mathematical problem to solve as we intend to reconstruct the shape of the interface using only the information about the volume fraction in a cell of interest and its nearest neighbours. Several piecewise reconstruction algorithms have been developed using finite difference methods as well as least squares methods [2], but they will not be discussed here for the sake of brevity as this is not the main focus of the project. As expected, the computational costs increase with the order of the method. A linear (second-order) reconstruction of an interface is shown in Figure 3.

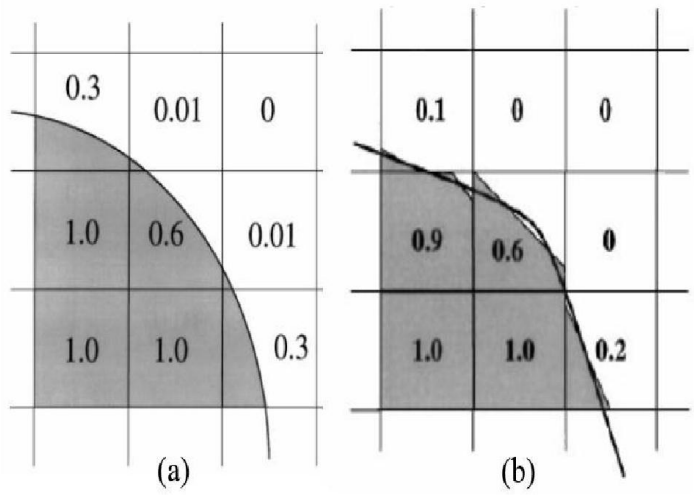

Figure 3: Piecewise linear reconstruction (b) of interface (a) [2]

This interfacial model is typically integrated into the continuity equation and Navier-Stokes equations, and the whole system is then solved using the material properties, boundary conditions and operating conditions supplied to the solver. However, it should be noted that VOF does have its set of advantages as well as drawbacks. It advantages include its effectiveness in mass conservation, its implicit recognition of topology (no special requirement for reconnection or breakup), the natural extension to higher dimensions, and ease of parallelization [2]. Furthermore, it maintains a very sharp (discontinuous) representation of the interface [8]. However, this means that it requires robust reconstruction algorithms and may sometime perform poorly in estimating local curvature, especially in cases involving high curvatures [8].

NUMERICAL METHOD

CASE 1: GRAVITY-DRIVEN FLOW

Consider the geometry in Figure 5, where a fluid fills the funnel nearly to the top initially and we would like to simulate the drainage process. In practice, the initial height of fluid in the funnel was approximately 14 cm to account for the diffuse nature of the interface when patching the registers in FLUENT; this was done for numerical stability reasons.

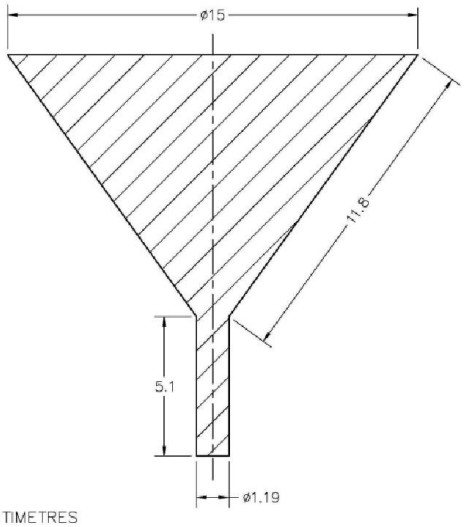

Figure 5: Schematic of funnel used for gravity-driven flow case

Simulation Assumptions:

1. Open system: $p_{in} = p_{out} = p_{atm}$ (101.325 kPa). p_{in} is applied at the boundary represented by the top face/edge and p_{out} is applied boundary represented by the bottom face/edge.
2. Walls: no-slip boundary condition.
3. Body forces: $g = -9.81\text{m/s}^2$ aligned with centre line of funnel (downward with respect to orientation of drawing).

Material properties (viscosity, density and surface tension) are given by those in Appendix A.

CASE 2: SIPHON

Consider the geometry in Figure 6, where the (inverted) funnel is incorporated into siphon system and the inlet is initially at a very high pressure relative to the outlet due to the hydrostatic head imposed on that side by the large tank filled with the tailings sample. It is important to note that the computational grid is only defined in the interior of the siphon (hatched pattern), and the effect of the applied pressure is incorporated in user-defined time-dependent pressure functions. In order to commence siphon action, the system must be primed; the simulation accounts for this by having the entire interior patched with fluid in its initial state. Subsequently, the pressure increases at the outlet and decreases in the inlet as fluid begins to empty in the large tank.

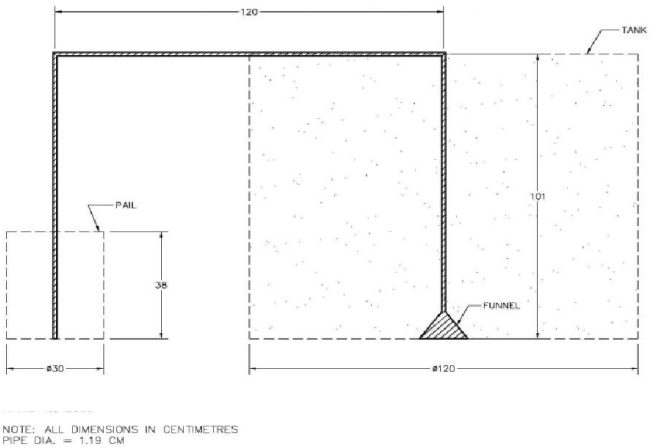

Figure 6: Schematic of siphon system used for tailings transfer

MESH GENERATION

The type of cells used in this work was exclusively hexahedral (3-D) or quad (2-D), completely avoiding tetrahedral (3-D) or triangular (2-D) elements. However, mesh quality is extremely critical for complex simulations to prevent divergence. There are several metrics used to evaluate the quality of a mesh such as Aspect Ratio (AR), EquiAngle Skew (EAS), size change, and others [10]. The two that were used in this work are defined below [11]:

$$Q_{AR} = \frac{\max\{e_i\}}{\min\{e_i\}}, \text{for } i = 1,\ldots,N \qquad (8)$$

$$Q_{EAS} = \max\left\{\frac{\theta_{max} - \theta_{eq}}{180^\circ - \theta_{eq}}, \frac{\theta_{eq} - \theta_{min}}{\theta_{eq}}\right\} \qquad (9)$$

where e_i is mean edge length in the local coordinate direction indexed by i, where N=2 for quadrilateral elements and N=3 for hexahedral elements, θ_{min} and θ_{max} are the minimum and maximum internal angles in the cell, and θ_{eq} is the internal angle in an equilateral cell (θ_{eq} = 90° for quadrilateral and hexahedral cells). Optimal values for Q_{AR} and Q_{EAS} are 1 and 0, respectively. As a general rule, "high-quality meshes contain elements that possess average EAS Q values of 0.1 (2-D) and 0.4 (3-D) [11]." For our application, EAS will be major criteria, at least initially, for judging quality as it is more crucial for simulation convergence.

Keeping these criteria in mind, consider the problem where we are required to construct the mesh for the full three-dimensional funnel. We use the method of volume decomposition [12] and mesh edge, then face, and then project to volume mesh in a bottom-up fashion [12,13]. This is a difficult problem from a geometric point of view, as the area shrinkage from the top to bottom face is an intrinsic characteristic of the object, and this introduces skew since we will be using a pure hex mesh and projection algorithm (Cooper) to extend the mesh from a source face to create the volume mesh (similar to an extrusion process) [10]. As visible from Figure 5, the diameter ratio α for the funnel is very large [10]:

$$\alpha = \frac{d_{\max}}{d_{\min}} = \frac{15\text{cm}}{1.19\text{cm}} \approx 12.6$$

Since we are restricted to using a projection method due to GAMBIT's limited hex meshing options, there is clearly no solution for reducing skew in the axial direction due to the narrowing nature of the object, we must at least take extreme care to minimize skew in the source face. As the source face is a circle (bottom face), the meshing problem now reduces to finding the optimal method for meshing a circle.

Several strategies are possible: a simplistic pave method, a decomposition into five logical rectangles with an inset square and a map scheme [10], or a decomposition into four logical triangles and a tri-primitive scheme. The results of these 3 strategies along with corresponding skew histograms (bin size = 0.1) are presented in Figure 7.

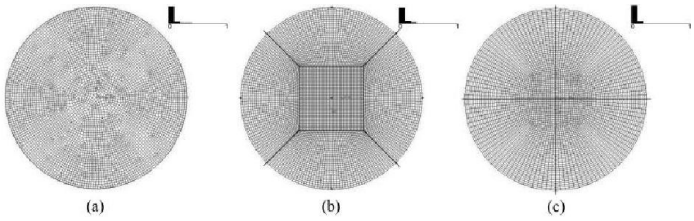

Figure 7: Schemes for paving a circle: pave (a), map (b), tri-primitive (c)

It is evident from Figure 7 that tri-primitive scheme offers the best skew distribution and the lowest maximum skew and it therefore the optimal choice. Through a process of trial-and-error, it was found that 50 intervals in the radial edge mesh and 30 intervals in circumferential edge mesh for each quadrant (a quarter of the circle) gave the best results for skew. This method is easy extended to three dimensions for cylinders and conical frustums.

The final mesh is presented in Figure 8a, after projection of the face mesh. Note that the mesh is especially fine at the region where the conical frustum meets the cylinder, as the flow behaviour in this region is expected to be critical.

The same mesh design principles discussed above were also applied to the 2-D test meshes prepared in this project. See Figure 8b, and 9 for the axi-symmetric funnel mesh and a close-up of the siphon mesh

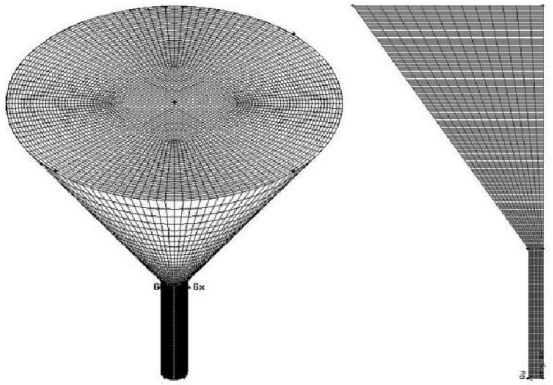

Figure 8: Optimized meshes for 3-D funnel (a), axisymmetric funnel (b)

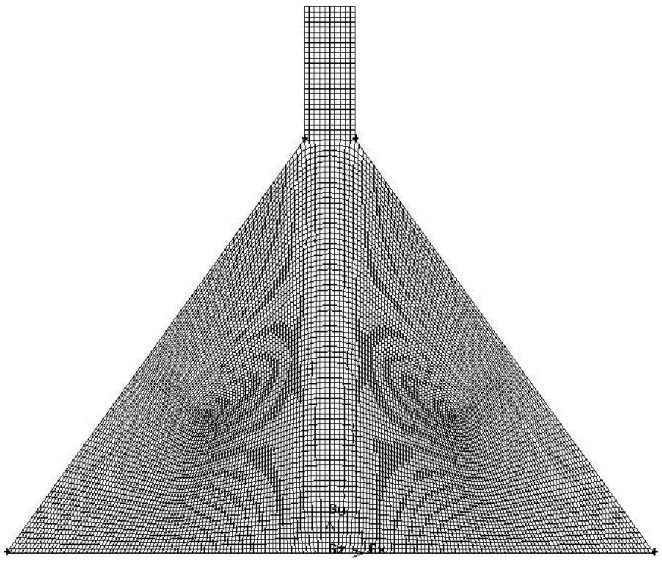

Figure 9: Optimized mesh for siphon

SOLUTION STRATEGIES

In this subsection, we will simply present the final solution settings used for the 2-D axi-symmetric gravity-driven flow simulation (this case was performed for testing the model before proceeding to 3-D), the full 3-D gravity-driven flow simulation, and the 2-D siphon simulation; these settings are listed in Table 1.

Table 1: Simulation solver settings

Setting	Axisymmetric gravity-driven flow	3-D gravity-driven flow	2-D siphon
Solver	pressure-based Navier-Stokes	pressure-based Navier-Stokes	pressure-based Navier-Stokes
Space	axisymmetric (no swirl)	3-D	2-D
Time formulation	unsteady	unsteady	unsteady
Flow regime	laminar	laminar	laminar
Multiphase	VOF, 2-phase	VOF, 2-phase	VOF, 2-phase
Pressure-velocity coupling	SIMPLE	SIMPLE	SIMPLE
Pressure discretization [14]	body-force weighted	body-force weighted	body-force weighted
Momentum discretization	first-order upwind	first-order upwind	first-order upwind
Volume fraction discretization	geo-reconstruct	geo-reconstruct	geo-reconstruct
Convergence criteria [15]	$\mathrm{Res}(\mathbf{v}_x, \mathbf{v}_y) \leq 10^{-3}$ $\mathrm{Res}(\text{continuity}) \leq 10^{-6}$	$\mathrm{Res}(\mathbf{v}_x, \mathbf{v}_y, \mathbf{v}_z) \leq 10^{-3}$ $\mathrm{Res}(\text{continuity}) \leq 10^{-6}$	$\mathrm{Res}(\mathbf{v}_x, \mathbf{v}_y) \leq 10^{-3}$ $\mathrm{Res}(\text{continuity}) \leq 10^{-6}$
Time step [10]	variable $\text{global(CFL)} = 2$ $dt_{min} = 10^{-5}$ s $dt_{max} = 10^{-3}$ s $\min\left\{\frac{dt_{i+1}}{dt_i}\right\} = 0.5$ $\max\left\{\frac{dt_{i+1}}{dt_i}\right\} = 2$	variable $\text{global(CFL)} = 2$ $dt_{min} = 10^{-5}$ s $dt_{max} = 10^{-2}$ s $\min\left\{\frac{dt_{i+1}}{dt_i}\right\} = 0.5$ $\max\left\{\frac{dt_{i+1}}{dt_i}\right\} = 2$	constant $dt = 10^{-4}$
Iterations	$\max\{\text{iterations}\} = 40$	$\max\{\text{iterations}\} = 40$	$\max\{\text{iterations}\} = 40$

Although the funnel has a high degree of symmetry, the shear effects arising due to the non-Newtonian properties of the tailings will only manifest themselves in the full 3-D simulation, with a potentially asymmetric flow and even the formation of small vortexes. The same arguments also apply to the siphon, but work on this case has just begun, so only a 2-D model is available at present for testing purposes. It is quite typical in CFD to test simpler models (often with lower dimensionality) and then progress to more complex models when the test cases are successful; this is the most reasonable methodology. Simulations are tracked with a surface monitor (e.g. average height of gas-liquid interface in gravity-driven flow) and are manually terminated at a meaningful end state for the system (e.g. when funnel is completely drained), or automatically terminated by floating-point errors caused by divergence of the simulation.

To begin with, we will discuss the reasons for the choices for settings that are common to all the simulations in Table 1. A pressure-based solver was used instead of a density-based solver because it is better suited for low-speed incompressible flows [16], and only a bulk density value was available as opposed to of density distribution (a requirement for the density-based solver) for the materials in this project. All of these simulations have unsteady formulations (also known as transient simulation) since we are interested in the time evolution of fluid properties, whether it be the draining of a funnel or the siphon action in the second case. Laminar flow is a natural assumption as the flows are low-speed and no significant turbulence is expected. The choice of the VOF multiphase model has already been discussed in Section 2.3, and it is apparent that there are two phases in the simulation: air (gas-phase) and tailings (liquid-phase). In terms of pressure-velocity coupling, SIMPLE (semi-implicit method for pressure-linked equations) was required as the pressure-based Navier-Stokes equations cannot be solved without the use of some approximations, and this comes in the form of iteratively solved

pressure and velocity correction equations which are substituted into other model equations for updates on fluid properties. The choice of SIMPLE is due to the lower computational cost compared to PISO (pressure-implicit with splitting of operators), which is far more intensive, but offers no noticeable advantage for multiphase flows [3]. The pressure discretization scheme was very important choice as these problems involve multiphase flows with large body forces (gravity) and perhaps strong swirling. For such applications, the body-force weighted strategy [14] is much more favourable compared to PRESTO! (pressure staggering option) as the body forces are known *a priori* [16]. Although second-order momentum is more accurate [15], the first-order was favoured due to the lower computational cost and concerns about the numerical stability of second-order differentials. Geo-reconstruct is the interfacial reconstruction methods native to VOF method and applied for this work. Residuals for velocity are at default values, but the continuity residual has been lowered three orders of magnitude due to the sensitivity of the VOF algorithm; these values are very important as they dictate if the simulation is judged as "converged" or "not converged" at any given flow time. Iterations simply represent the marching of the solver in other (non-time) dimensions, and the default maximum value of 20 was doubled for increased spatial accuracy of the results.

The simulations were performed with a smaller time step as it is already more computationally intensive due to its three-dimensional nature and this is an effort to reduce the cost. Early simulations of the siphon simulation were performed with a fine temporal resolution (10^{-4} s) as the simulation is very unstable and easily diverges. To improve this even further, one could start the simulation at even finer resolutions (10^{-6} s) and increase the time step size as the residuals begin to stabilize.

VISUALIZATION SCHEMES

Our proposed scheme for our visualization of the gravity-driven case involves splitting the funnel with radial planes at various angles and displaying different properties on various pieces of the model. Limited visualization results are available for the siphon yet, so we will only discuss results for the first case.

As the time-evolution of the interface is especially important for evaluating the results of the simulation, one half of the funnel was devoted to displaying the volume fraction ϕ of the secondary phase (in this case, the tailings) with an overlay of the velocity vectors (along streamlines) with proportionally sized and appropriately coloured arrows. The other half of the funnel was divided into quarters (45° span for each section) and these pieces were devoted to displaying interpolated contour maps of pressure (Pa), velocity magnitude (m/s), wall shear (Pa), and vorticity ($\nabla \times \mathbf{v}$) magnitude (1/s) respectively. Transparency features were utilized appropriately on the various sections to maximize the visibility of all pieces of the structure and also different colour maps for different properties to avoid any ambiguity. Figure 10 shows a representative visualization result for the settling in a funnel geometry (the pressure given is the static gauge pressure).

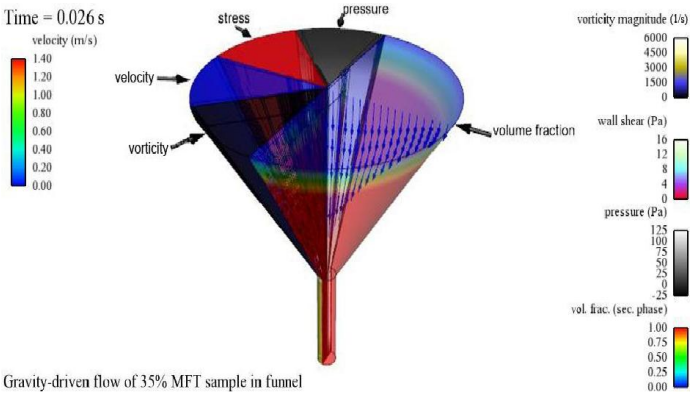

Figure 10: Representative visualization scheme for MFT settling

RESULTS AND ANALYSIS

CASE 1: GRAVITY-DRIVEN FLOW

MFT (35% solids content) gravity driven simulation is used in this work. This representative MFT is chosen by examining the progression of the untreated fluids from visco-plastic fluid with $n > 1$ to Bingham plastics ($n = 1$) and the increase of the yield stress τ_0 with increasing solids content. Additionally, the slope m for MFT increases within the Bingham plastics with solids contents. See Appendix A for details.

TIME EVOLUTION OF THE GAS-LIQUID INTERFACE

To begin with, we examine the interface development as time progresses to confirm if the funnel is draining realistically. Figure 11 shows the iso-surfaces of $\phi = 0.5$ (the best numerical representation of the shape of the interface) in the cross-sectional plane at various flow times. The times are not evenly spaced due to the discrepancy caused by using a variable time stepping scheme and a data save frequency given by a constant number of time steps.

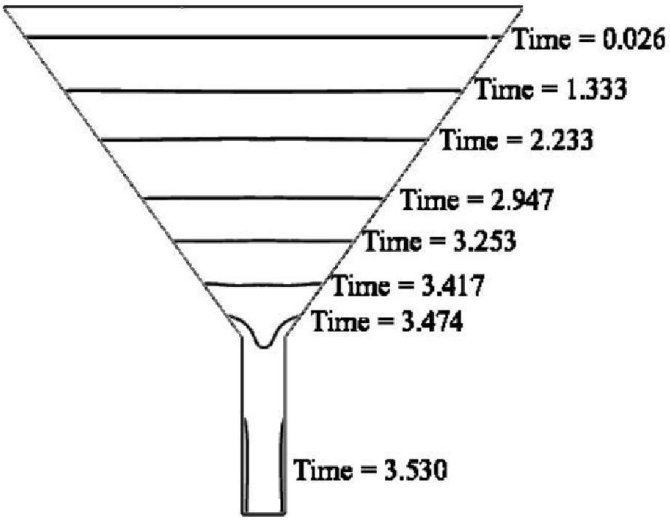

Figure 11: Iso-surfaces of $\phi = 0.5$ in the cross-sectional plane at various flow times

From close examination of Figure 11, it is apparent that the shape of the interface is quite flat until it reaches the cylindrical part of the funnel. This change in geometry clearly alters the flow conditions as it forces the fluid from a gradually narrowing "pipe" (frustum) into a constant diameter "pipe" (cylinder). The fluid accelerates rapidly through this small cross section. However, some very unphysical effects such as wall adhesion of thick layers and wave-like menisci were showing up in this cylindrical region before the variable time step was employed. In this corrected simulation, we can see that only a thin layer of fluid remains adhered to the walls instants before complete drainage (t = 3.530 s), which is quite realistic.

Ideally, the model is most effectively evaluated with an experimental value of drain time. Unfortunately, these experimental values are not yet available, so the best possible comparison for the time-dependent behaviour is to a theoretical drain curve, given the same geometry, for an incompressible fluid obeying Torricelli's law.

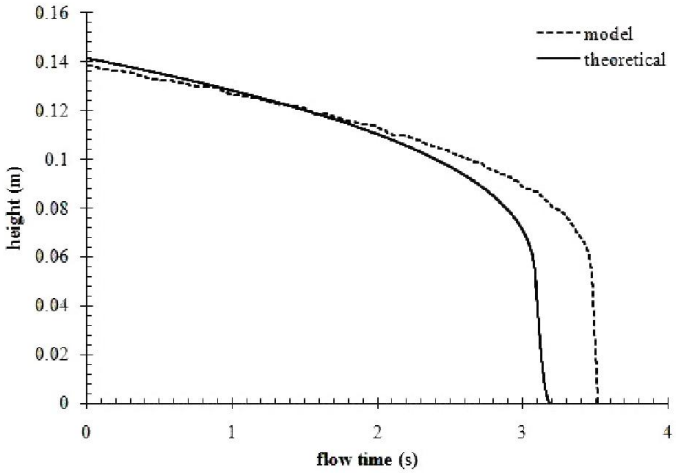

Figure 12: Comparison of model (35% MFT) and theoretical drain curves for the funnel geometry

Note that the theoretical calculation was modified to account for the fact that the funnel was only filled initially to the height of about 14 cm, measured from the outlet of the funnel. It is clear that the two curves show excellent agreement until about 2.2 s, but begin to rapidly diverge after that point. It is interesting to note that the model curve is somewhat noisy compared to the smooth progression of the theoretical curve. This "noise" arises from the fact that the interface displayed slight undulations as it drained. These were captured in the height function, since it was defined, through a surface monitor, as the vertex average of the ϕ = 0.5 iso-surface on the funnel symmetry axis with respect to flow time. The most important similarity between the curves is their overall shape, and one can easily recognize the transition from the gentle slope of the frustum to the sharp falloff in cylinder, which occurs at approximately 3.1 s in the theoretical curve and a little after 3.4 s in the model curve. These are expected characteristics of a funnel geometry, so the existence of them in both curves is a promising sign.

Next, we can proceed to calculate an error percentage ε between the curves for the total drain time:

$$\varepsilon = \left\| \frac{t_{f,model} - t_{f,theo}}{t_{f,theo}} \right\| \times 100\% \approx \left\| \frac{3.5\text{s} - 3.2\text{s}}{3.2\text{s}} \right\| \times 100 = 9.375\%$$

This is a fairly low accuracy (< 10%,) and multiphase CFD simulations can be attributed to the inherent numerical complexity. Also, the theoretical calculation ignores effects such as density, viscosity, and surface tension, all of which as incorporated into the FLUENT simulation; these may very well be the reasons for the increasing discrepancies at larger flow times. But until further data becomes available, this is the best possible evaluation at this time.

NON-NEWTONIAN FLOW BEHAVIOR OF OIL SANDS MFT

Representative hydrodynamics of oil sands MFT (pressure, velocity, wall shear, vorticity) at one instance of time (t = 3.474 s) when the flow becomes critical (i.e. when interface reaches the region between frustum and cylinder is presented. Figure 13 shows the results in the cross-sectional plane (the black lines in Figures 13 a, b, and c are the iso-surfaces of ϕ = 0.5 at the given time).

From Fig. 13(a), it is clear that the fluid is accelerating, and that the trough of the interface is moving downwards fastest. The pressure increases towards the bottom of the cylinder, as expected, due to the hydrostatic head. Fig. 13(b) shows that the wall shear reaches a maximum of about 25 Pa, at the corner vertex. This is expected as the transition between frustum and cylinder is sharp, with no smoothing (i.e. fillets/chamfers) applied. Lastly, Fig. 13(c) shows the formation of two small symmetrical vortices centred on the line separating frustum and cylinder. This is also quite typical as swirling may occur at sharp transitions to a constant diameter "pipe."

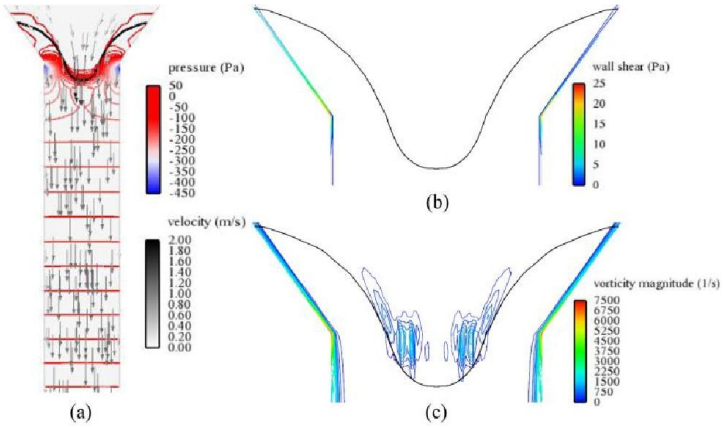

Figure 13: Velocity field superimposed on pressure contours (a), contours of wall shear (b), and contours of vorticity (c)

CASE 2: SIPHON

The siphon geometry was also simulated a s a component of the overall transfer process using MFT properties. Figure 14 shows the flow field at siphon intake 1 s after initialization. As is visible, the velocity vectors point upwards, and are being accelerated into the cone-structure due to the large pressure difference between inlet and outlet. As a result the simulation is complete when the outlet pressure reaches 4.6 kPa.

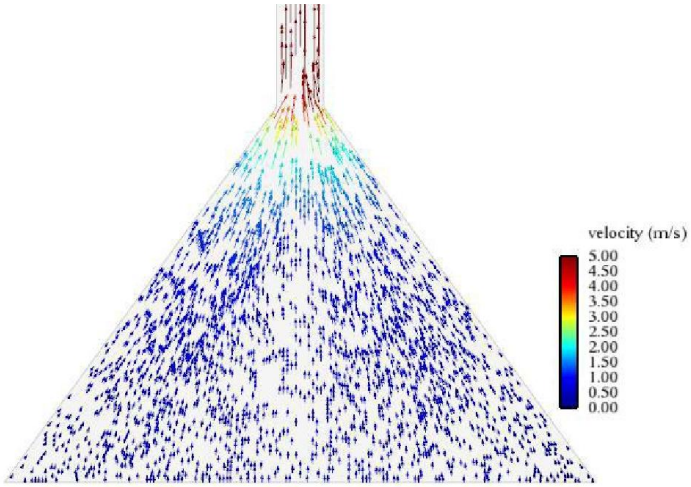

Figure 14: Siphon flow field at intake at t=1 s

CONCLUDING SUMMARY

Flow behaviour of oil sands tails was examined in funnel shaped geometries with the goal of developing a new transfer facility for addition of partially processed tailings to the tailings ponds without disturbing the settled tailings.

An understanding of the flow behaviour with MFT containing 35% solids was obtained from the CFD simulations of the funnel and siphon. The velocity in the funnel (gravity driven flow) peaks at the end of the cone while in the siphon the velocity will continue to increase through the cylindrical section. Also maximum shear rate and the formation of small vortices is obtained close to the transition in the geometry from the cone to the cylinder in both funnel and siphon geometries indicating the need to develop rigorous models to predict this transition.

With regards to future possibilities, the progress made so far on the funnel and additional studies on the siphon and other geometries is expected to improve the understanding of settling dynamics of oil sands tailings and in improving existing methods or designing new methods for tailings transfer processes.

ACNOWLEDGEMENTS

This project was funded by the Canadian PERD-Oil sands program. The authors would like to thank Akash Ravi (Coop student) for his support during this project.

REFERENCES

[1] R. P. Chhabra, *Bubbles, Drops, and Particles in Non-Newtonian Fluids*. CRC Press, 2007.

[2] R. Scardovelli and S. Zaleski, "Direct numerical simulation of free-surface and interfacial flow," *Annual Review of Fluid Mechanics*, vol. 31, pp. 567-603, 1999.

[3] V. V. Ranade, *Computational Flow Modeling for Chemical Reactor Engineering*, vol. 5 of *Process Systems Engineering Series*. Academic Press, 2002.

[4] N. N. Suthaker and J. D. Scott, "Thixotropic strength measurement of oil sand fine tailings," *Canadian Geotechnical Journal*, vol. 34, pp. 974-984, 1997.

[5] *Tailings and Mine Waste 1998*. Taylor & Francis, 1 ed., January 1998.

[6] H. J. Weber and G. B. Arfken, *Essential Mathematical Methods for Physicists*. Academic Press, 2003.

[7] T. Cebeci, J. P. Shao, F. Kafyeke, and E. Laurendeau, *Computational Fluid Dynamics for Engineers*. Springer, 2005.

[8] W. B. J. Zimmerman, *Process Modelling and Simulation with Finite Element Methods*, vol. 15 of *Series on Stability, Vibration and Control of Systems*. World Scientific Publishing, 2004.

[9] C. W. Hirt and B. D. Nichols, "Volume of fluid (vof) method for the dynamics of free boundaries," *Journal of Computational Physics*, vol. 39, pp. 201-225, 1981.

[10] A. Ravi, J. Abanto, G. Li, and H. Metwally, "Simulation of a funnel using vof (clarify esupport case 76613)." February 2009.

[11] Fuent Inc., *GAMBIT 2.4 User's Guide*, May 2007.

[12] Fluent Inc., *Volume Meshing*, Introductory GAMBIT Training, Fluent Inc., June 2006.

[13] Fluent Inc., *Edge and Face Meshing*, Introductory GAMBIT Training, Fluent Inc., June 2006.

[14] A. Ravi and H. Metwally, "Vof: how to monitor the free surface and its profile with time (clarify esupport case 77057)." March 2009.

[15] A. Ravi and H. Metwally, "Vof for herschel-bulkley fluid draining from a funnel (clarify esupport case 77711)." March 2009.

[16] Fluent Inc., *FLUENT 6.3 User's Guide*, September 2006.

[17] M. R. Spiegel, *Schaum's Outline of Theory and Problems in Probability and Statistics*. McGraw-Hill, 1998.

[18] C. Angle, R. Zrobok, and H. Hamza, "Surface properties and elasticity of oil-sands derived clays found in a sludge pond," *Applied Clay Science*, vol. 7, pp. 455-470, 1993.

[19] R. Darby, *Chemical Engineering Fluid Mechanics*. Marcel Dekker, Inc., 2 ed., 2001.